JACS
JOURNAL OF THE AMERICAN CHEMICAL SOCIETY
Article
Cite This: J. Am. Chem. Soc. 2018, 140, 2115−2126
pubs.acs.org/JACS

Probing Conformational Exchange in Weakly Interacting, Slowly Exchanging Protein Systems via Off-Resonance $R_{1\rho}$ Experiments: Application to Studies of Protein Phase Separation

Tairan Yuwen,[†] Jacob P. Brady,[†] and Lewis E. Kay*[,†,‡]

[†]Departments of Molecular Genetics, Biochemistry and Chemistry, University of Toronto, Toronto, Ontario, Canada M5S 1A8
[‡]Hospital for Sick Children, Program in Molecular Medicine, Toronto, Ontario, Canada M5G 1X8

Supporting Information

ABSTRACT: $R_{1\rho}$ relaxation dispersion experiments are increasingly used in studies of protein dynamics on the micro- to millisecond time scale. Traditional $R_{1\rho}$ relaxation dispersion approaches are typically predicated on changes in chemical shifts between corresponding probe spins, $\Delta\omega_{GE}$, in the interconverting states. Here, we present a new application of off-resonance ^{15}N $R_{1\rho}$ relaxation dispersion that enables the quantification of slow exchange processes even in the limit where $\Delta\omega_{GE} = 0$ so long as the spins in the exchanging states have different intrinsic transverse relaxation rates ($\Delta R_2 = R_{2,E} - R_{2,G} \neq 0$). In this limit, the dispersion profiles become inverted relative to those measured in the case where $\Delta\omega_{GE} \neq 0$, $\Delta R_2 = 0$. The theoretical background to understand this effect is presented, along with a simplified exchange matrix that is valid in the limits that are germane here. An application to the study of the dynamics of the germ granule protein Ddx4 in a highly concentrated phase-separated state is described. Notably, exchange-based dispersion profiles can be obtained despite the fact that $\Delta\omega_{GE} \approx 0$ and ΔR_2 is small, ~20−30 s^{-1}. Our results are consistent with the formation of a significantly populated excited conformational state that displays increased contacts between adjacent protein molecules relative to the major conformer in solution, leading to a decrease in overall motion of the protein backbone. A complete set of exchange parameters is obtained from analysis of a single set of ^{15}N off-resonance $R_{1\rho}$ measurements recorded at a single static magnetic field and with a single spin-lock radio frequency field strength. This new approach holds promise for studies of weakly interacting systems, especially those involving intrinsically disordered proteins that form phase-separated organelles, where little change to chemical shifts between interconverting states would be expected, but where finite ΔR_2 values are observed.

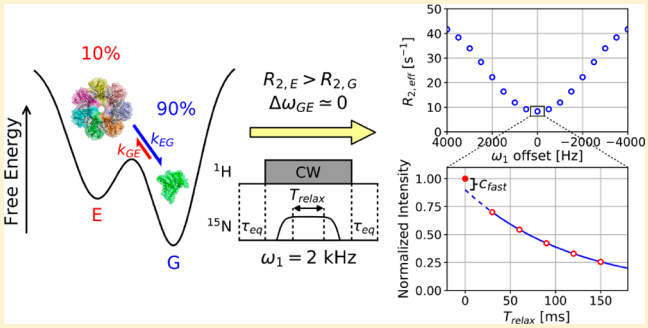

INTRODUCTION

The dynamics of biomolecules are complex and often integral to function, spanning a wide range of time scales and involving the interconversion between different conformers.[1] As such, a detailed understanding of how motion regulates the ways in which biomolecules perform their tasks becomes critical and an atomic-level description of the conformers that are explored through dynamics has become an important goal of molecular biophysics. Often, many of the conformers are only transiently formed and sparsely populated so that they are invisible to many of the traditional biophysical approaches that have been developed over the years. NMR spectroscopy has emerged as a powerful tool for studies of biomolecular dynamics spanning many orders of magnitude, including cases involving the interconversion between highly populated and long-lived conformers (so-called ground states) and sparsely populated and transiently formed conformers (excited states), the latter of which cannot be observed directly.[2] Of particular interest in the past decade has been the study of motions on the micro- (μs) to millisecond (ms) time scale, as these are often functionally relevant. A variety of spin-relaxation methods have emerged to pursue such studies and all have strengths as well as potential drawbacks. For example, a prerequisite for $R_{1\rho}$,[3] Carr−Purcell−Meiboom−Gill (CPMG)[2a] and chemical exchange saturation transfer (CEST)[4] based experiments is the presence of significant chemical shift differences ($\Delta\omega$) for the NMR-active nuclei that report on the interconversion between states. In contrast, shift differences are not needed for dark state exchange transfer (DEST) spectroscopy,[5] replaced by the requirement for large differences in transverse relaxation rates between interconverting spins (ΔR_2). Simulated profiles from each class of experiment are highlighted in Figure 1 for limiting cases where either $\Delta\omega_{GE} = 0$ or $\Delta R_2 = 0$.

Although there are many examples of interconverting systems with substantial changes in chemical shifts or relaxation rates that are amenable to study using the approaches mentioned above, this is not universally the case by any

Received: September 7, 2017
Published: January 5, 2018

DOI: 10.1021/jacs.7b09576
J. Am. Chem. Soc. 2018, 140, 2115−2126

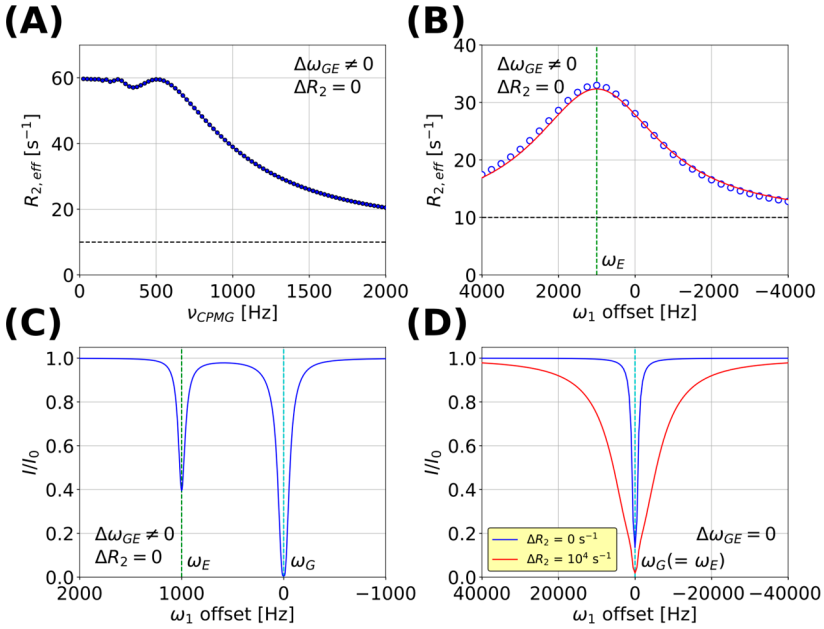

Figure 1. Spin-relaxation experiments for quantifying conformational exchange processes. Numerical simulations of profiles expected from (A) CPMG, (B) off-resonance $R_{1\rho}$, (C) CEST, and (D) DEST analyses. All simulations were performed with the following parameters: $p_E = 0.10$, $R_1 = 0$ s^{-1}, $R_{2,G} = 10$ s^{-1}. Panel (A) is simulated with $k_{ex} = 500$ s^{-1}, $\Delta\omega_{GE}/(2\pi) = 1000$ Hz, $\Delta R_2 = 0$ s^{-1}. Panel (B) is simulated with $k_{ex} = 1000$ s^{-1}, $\Delta\omega_{GE}/(2\pi) = 1000$ Hz, $\Delta R_2 = 0$ s^{-1} and a B_1 field strength of 2000 Hz. The blue circles and red curve are obtained from the numerical simulation and eq 10, respectively. In both panels (A) and (B), the horizontal black dashed line is obtained by setting $\Delta\omega_{GE} = 0$ in the simulations. In panel (C), the CEST profile is calculated with $k_{ex} = 50$ s^{-1}, $\Delta\omega_{GE}/(2\pi) = 1000$ Hz, $\Delta R_2 = 0$ s^{-1}, $T_{Ex} = 0.2$ s, and a B_1 field strength 30 Hz. The smaller of the two dips disappears in the limit that $\Delta\omega_{GE} = 0$. Parameters used to simulate panel (D) are $k_{ex} = 50$ s^{-1}, $\Delta\omega_{GE}/(2\pi) = 0$ Hz, $T_{Ex} = 0.4$ s, B_1 field strength 300 Hz, and $\Delta R_2 = 0$ or 10000 s^{-1}. The cyan and green dashed lines denote the position of ground and excited states, respectively.

means. One example of note that we are currently pursuing involves the intrinsically disordered domain from the Ddx4 protein, Ddx4$_{1-236}$. Ddx4 is specific to germ cells and the major component of a membraneless organelle in the cytoplasm of spermatocytes and spermatids.[6] Ddx4$_{1-236}$ phase separates to form a highly condensed phase with a protein concentration of approximately 400 mg/mL,[7] and it is of interest to understand the molecular basis by which this process occurs. More generally, an atomic level description of the various ways by which proteins and nucleic acids phase separate has become critical because phase separation leads to the formation of a variety of different membrane-less organelles in the cell that are involved in the regulation of different biological processes that are essential to proper cellular function.[8]

In an effort to take the first steps toward understanding phase separation of Ddx4$_{1-236}$, we initially recorded CPMG relaxation dispersion experiments to quantify interactions between monomers in the condensed phase. In this class of experiment transverse relaxation rates, $R_{2,eff}$, are recorded as a function of the number of chemical shift refocusing pulses, proportional to ν_{CPMG} in Figure 1A, that are applied in an interval of fixed duration.[2a,9] Effective $|\Delta\omega_{GE}|$ values decrease as a function of increasing numbers of pulses, leading to a decrease in R_2 rates. The resulting so-called relaxation dispersion profiles ($R_{2,eff}$ vs ν_{CPMG}) can, in turn, be fit to models of chemical exchange to extract exchange parameters and $|\Delta\omega_{GE}|$ values, providing insight into the sparse conformers that are formed.[2a,10] In the case of Ddx4$_{1-236}$, however, relaxation rates showed little variation with numbers of pulses, consistent with small chemical shift differences between nuclei in the exchanging states or with exchange time scales that are outside the ~500−2500 s^{-1} exchange regime that is typically monitored by this class of experiment, and thus, they could not be analyzed rigorously without additional input data. ^{15}N off-resonance $R_{1\rho}$ experiments were also recorded in which the decay of spin-locked magnetization is measured, in an effort to quantify chemical exchange processes that might be occurring. Off-resonance $R_{1\rho}$ measurements are particularly useful for the characterization of exchange processes where rates of interconversion are significantly larger than those quantified by CPMG methodology.[3] Figure 1B illustrates the types of profiles that are generally obtained from such experiments, focusing on the moderate to slow chemical exchange regime where the exchange rates are on the order of $|\Delta\omega_{GE}|$. In this case, the resulting $R_{2,eff}$ vs radio frequency (RF) offset dispersion profile has a maximum at the resonance frequency of the minor state peak, ω_E.[11] Notably, as described below, $R_{2,eff}$ dispersion profiles having this form were not observed in studies of Ddx4$_{1-236}$. Instead, "inverted" profiles were obtained that, to our knowledge, have not been previously reported experimentally. We could not explain these profiles assuming an exchanging system in the limit that $\Delta R_2 = 0$, a condition that is most often invoked in theoretical analyses of $R_{1\rho}$ experiments and in fits of experimental data. The unexpected form of the experimental data was intriguing, prompting a detailed analysis that focuses on the potential of this class of experiment to provide heretofore unappreciated insights into the dynamics of sparsely populated conformational states, in general, including a specific application to the Ddx4$_{1-236}$ phase-separating system that we have been studying.[7b]

To this end, we present a simple theoretical description of the $R_{1\rho}$ experiment in the limit where $\Delta R_2 \neq 0$ that provides an intuitive feel for how the "inverted" profiles measured for Ddx4$_{1-236}$ arise. We show that quantifiable profiles can be obtained, even in the case where $\Delta\omega_{GE} = 0$ and for ΔR_2 values that are reasonably small, 20−40 s^{-1}, so long as the exchange

DOI: 10.1021/jacs.7b09576
J. Am. Chem. Soc. 2018, 140, 2115−2126

between conformers, k_{ex}, is on the order of or smaller than ΔR_2 and we present a procedure for extracting k_{ex} and per-residue ΔR_2 rates from $R_{1\rho}$ experiments recorded at single static and B_1 fields. An application to Ddx4$_{1-236}$ is presented, showing that in the condensed phase-separated state of the protein a populated minor conformer is formed, in addition to the ground state, where the backbone motions are reduced. Through both simulations and experimental results obtained on the Ddx4 system we highlight that the ^{15}N $R_{1\rho}$ experiment provides access to an exchange regime that is not easily amenable to other classes of spin relaxation experiment. It is anticipated that such $R_{1\rho}$ studies will find important applications in quantifying exchange processes driven by formation of weak molecular contacts such as those involving intrinsically disordered proteins (IDPs) where only very small shift differences would be expected but where small, but measurable ΔR_2 values might be found.

MATERIALS AND METHODS

Sample Preparation. Wild-type human Ddx4$_{1-236}$ (referred to in what follows as Ddx4) and a mutant that does not phase separate where all 14 Phe residues were replaced by Ala, Ddx4$_{14FtoA}$, were expressed and purified as described previously.[7] As discussed in a previous publication,[7b] wild-type Ddx4$_{1-236}$ spontaneously phase separates to form condensed and dilute phases with protein concentrations of 380 and 7 mg/mL (30 °C), respectively. In contrast, samples of Ddx4$_{14FtoA}$ do not phase separate (except at 0 °C) and high protein concentrations (370 mg/mL) could only be achieved through extensive centrifugation. After purification, unlabeled samples were doped with 10% [U-^{15}N,^{13}C]-labeled protein to facilitate NMR analysis. NMR samples of phase-separated Ddx4 and highly concentrated Ddx4$_{14FtoA}$ were prepared by dialysis into buffer containing 20 mM sodium phosphate, 100 mM NaCl, 5 mM TCEP, 90% H_2O/10% D_2O, pH 6.5, transferred into 3 mm NMR tubes (Wilmad), gently centrifuged, then allowed to equilibrate at 30 °C for a minimum of 24 h to ensure that the condensed droplets coalesce to a homogeneous phase. In the case of Ddx4$_{1-236}$ care was taken to ensure that the condensed phase filled the NMR coil volume and beyond, with the dilute phase (that is easily identified as being above the condensed region) removed prior to experiments. A sample of the B1 domain of peptostreptococcal protein L (referred to as protein L in what follows) was prepared as described previously[12] and used as a control to test the experiments. Protein L concentrations were 4.0 or 1.5 mM for [U-^{2}H,^{15}N]- or [U-^{15}N,^{13}C]-labeled samples, respectively, dissolved in buffer comprising 50 mM sodium phosphate, 0.05% NaN_3, 90% H_2O/10% D_2O, pH 6.0.

NMR Spectroscopy. Off-resonance ^{15}N $R_{1\rho}$ data sets were recorded on Ddx4 samples (pulse scheme of Figure 4) using an 800 MHz Bruker spectrometer equipped with a cryogenically cooled probe with a z-axis pulsed field gradient, 30 °C. Experiments were obtained as pseudo-4D data sets whereby spectra with three T_{relax} values of 50, 100, and 150 ms were measured for each offset spanning the range of [−4000, 4000] Hz from the center of the ^{15}N spectral region (118 ppm), in step sizes of 250 Hz. The values of $T_{relax,max}$ and τ_{eq} were set to 160 and 50 ms, respectively. In addition, a reference 2D plane was measured for T_{relax} = 0, where the ^{15}N spin-lock and adiabatic half passage pulses (AHPs) are not applied during the $T_{relax,max}$ period (see Figure 4) so that magnetization resides continuously along the z-axis. The RF field strength for the ^{15}N spin-lock was set to approximately 2 kHz, and calibrated according to the relative sizes of the apparent one-bond ^{1}H−^{15}N scalar couplings in the presence or absence of ^{15}N continuous wave decoupling during acquisition.[3] Each 2D data set was recorded with 2 transients/FID, a relaxation delay of 3.0 s and (768, 90) complex points in (t_2, t_1) to give a net acquisition time of ∼20 min/spectrum. The net measurement time for each complete off-resonance ^{15}N $R_{1\rho}$ data set was approximately 35 h.

Off-resonance ^{15}N $R_{1\rho}$ data sets were recorded on protein L samples using a 600 MHz Bruker spectrometer equipped with a triple gradient axis cryogenically cooled probe, 25 °C. The ^{15}N spin-lock RF field strength, T_{relax} and ^{15}N offset values were similar to those used in measurements on Ddx4 samples. Each 2D data set was recorded with 2 transients/FID, a relaxation delay of 3.0 s, and (640, 64) complex points in (t_2, t_1) to give a net acquisition time of ∼12 min/spectrum. The net measurement time for each $R_{1\rho}$ data set was ∼21 h.

^{15}N CEST experiments were recorded on the condensed phase of phase-separated Ddx4 using a pulse scheme described previously,[4] with weak B_1 field strength of 27.0 Hz and T_{Ex} = 400 ms. The net measurement time was ∼22 h. ^{15}N CPMG experiments were recorded on the same sample using the CPMG experiment of Yang and colleagues.[13] The duration of the constant time CPMG period was set to 100 ms, with 25 ν_{CPMG} values sampled in the range of 10−400 Hz, where $\nu_{CPMG} = 1/(2\delta)$, and δ is the time between successive refocusing pulses. Note that the (largely unlabeled) sample used was doped with 10% [U-^{15}N,^{13}C]-labeled protein. Thus, during the long CPMG relaxation element ^{15}N magnetization evolves from one- and two-bond ^{15}N−^{13}C couplings to produce antiphase components that relax more rapidly than in-phase magnetization, leading to small (1−2 s^{-1}) spurious dispersion profiles. This effect was eliminated by the application of ^{13}C adiabatic pulses during δ (every 5 ms). A net measurement time of 12 h was used for each CPMG data set.

Data Analysis. All NMR spectra were processed and analyzed using the NMRPipe suite of programs[14] with peak intensities extracted with the *autofit* subroutine. For the analysis of off-resonance ^{15}N $R_{1\rho}$ data sets, $R_{1\rho} - R_1$ rates for each offset were obtained from fits of the decay of peak intensities (recorded with data sets measured with T_{relax} = 50, 100, and 150 ms; the reference data set with T_{relax} = 0 was excluded). Actual T_{relax} values (except for T_{relax} = 0) used for the curve fitting were corrected for the duration of the AHP pulses applied prior to and after each spin-lock period (see the Supporting Information). The parameter, c_{fast}, was obtained as the difference between normalized intensities of the extrapolated single exponential decay fit (based on T_{relax} = 50, 100, and 150 ms) to T_{relax} = 0 and the reference with T_{relax} = 0 (see text). Uncertainties of $R_{1\rho} - R_1$ rates and c_{fast} values were estimated from Monte Carlo analyses using 1000 repeats,[15] with the signal-to-noise ratio of peaks evaluated from the peak signal intensity divided by the average random spectral noise. The uncertainties in $R_2 - R_1$ values were propagated from the uncertainties in the $R_{1\rho} - R_1$ rates according to $\sigma_{R2-R1} = \sigma_{R1\rho-R1}/\sin^2\theta_G$ (where θ_G is the angle between the spin locked ground-state magnetization and the z-axis). Exchange parameters (p_E, k_{ex}) were obtained from global fits of R_2 and c_{fast} offset profiles by minimizing a χ^2 function according to the analytical equations described in the text and assuming that the ^{15}N chemical shift differences between corresponding spins in the ground and excited states are 0, an assumption justified by ^{15}N CPMG experiments. In total 26 Ddx4 residues with significant R_2 relaxation dispersion profiles (see text) were selected for estimation of exchange parameters (p_E, k_{ex}) and calculation of the χ^2 surface. The fitting parameters include residue specific ΔR_2 (= $R_{2,E} - R_{2,G}$) values, where $R_{2,i}$ is the intrinsic transverse relaxation rate of a spin in state i ($i \in \{G,E\}$), and $R_{2,G} - R_1$ values, with (p_E, k_{ex}) treated as global parameters. Once (p_E, k_{ex}) values were established they were fixed and per-residue fits of the remaining dispersion profiles allowed the extraction of ΔR_2 and $R_{2,G} - R_1$ rates (for 86 residues). A similar analysis was performed for data recorded on Ddx4$_{14FtoA}$.

CPMG relaxation dispersion profiles of Ddx4 were fit to a two-site chemical exchange model using the software program ChemEx.[16] Values of (p_E, k_{ex}, ΔR_2) that were obtained from analysis of $R_{1\rho}$ data were enforced and $|\Delta\varpi_{GE}|$ extracted for the 86 residues that were analyzed.

RESULTS AND DISCUSSION

Probing Exchange in Systems with $\Delta R_2 \neq 0$ via ^{15}N Off-Resonance $R_{1\rho}$ Experiments. The theoretical basis underlying "traditional" $R_{1\rho}$ relaxation dispersion experiments has been well established in the literature.[3] In the description that follows we consider a simple two-state exchange process,

DOI: 10.1021/jacs.7b09576
J. Am. Chem. Soc. 2018, 140, 2115−2126

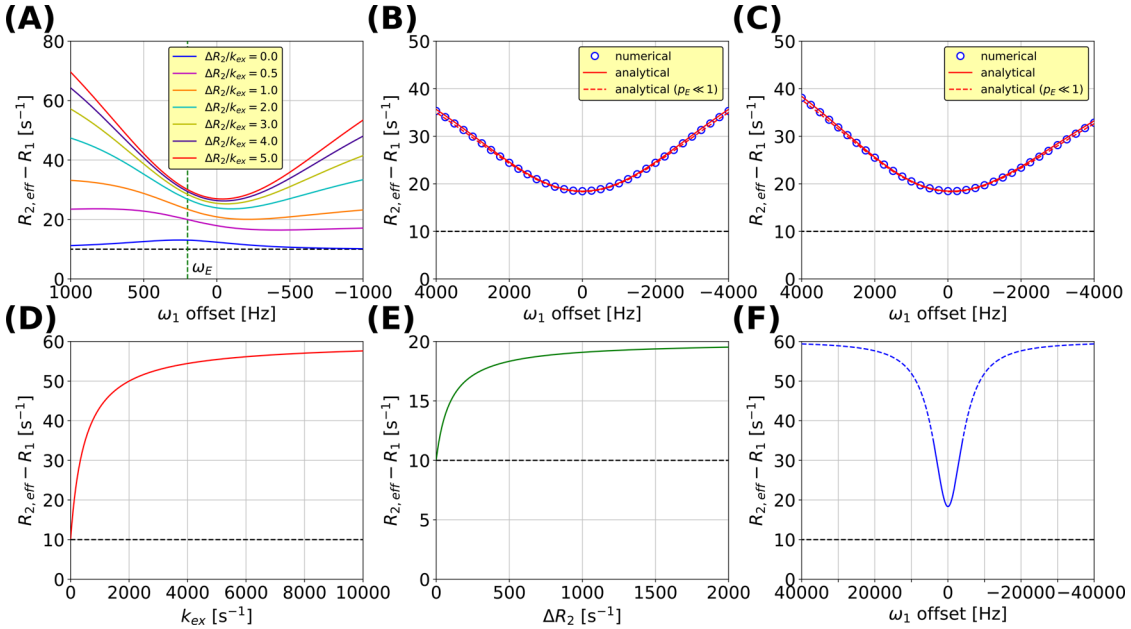

Figure 2. Off-resonance $R_{1\rho}$ profiles are highly dependent on the $\Delta R_2/k_{ex}$ ratio. (A–C) Simulated ^{15}N R_2 vs ω_1 offset profiles. (A) p_E = 0.10, k_{ex} = 200 s^{-1}, R_1 = 0 s^{-1}, $R_{2,G}$ = 10 s^{-1}, $\Delta\omega_{GE}/(2\pi)$ = 200 Hz and B_1 field strength of 500 Hz; ΔR_2 values up to 1000 s^{-1} are shown to illustrate the transition of the curve from concave, the traditional shape in the limit where $\Delta\omega_{GE} \neq 0$, $\Delta R_2 = 0$ (blue) to convex (red). The dashed green line indicates the resonance position of the spin in the excited state. (B–C) p_E = 0.10, k_{ex} = 100 s^{-1}, R_1 = 0 s^{-1}, $R_{2,G}$ = 10 s^{-1}, ΔR_2 = 500 s^{-1}, B_1 field strength of 2000 Hz, $\Delta\omega_{GE}/(2\pi)$ = 0 (B) or 500 Hz (C). The B_1 inhomogeneity is assumed to be 10%, simulated as described previously.[4] Solid and dashed lines in red are obtained from analytical equations without (for example, eq 4) or with (eqs 8 and 9) the assumption of $p_E \ll 1$. Numerical simulations (blue circles) made use of the complete 6 × 6 Bloch–McConnell exchange matrix that is relevant in the case of 2-site chemical exchange. (D–F) p_E = 0.10, R_1 = 0 s^{-1}, $R_{2,G}$ = 10 s^{-1}, $\Delta\omega_{GE}$ = 0 and B_1 field strength = 2000 Hz with ΔR_2 = 500 s^{-1} in (D), k_{ex} = 100 s^{-1} in (E); calculations assumed that the measurement is carried out on-resonance ($\sin^2\theta = 1$). The profile in panel (F) is simulated with k_{ex} = 100 s^{-1}, ΔR_2 = 500 s^{-1}, a B_1 field strength of 2000 Hz over an offset range of [−40000, 40000] Hz; the solid curve denotes the region that is typically measured experimentally. The black dashed lines indicate $R_{2,eff} - R_1$ rates in the absence of the slow-exchange process.

G $\underset{k_{EG}}{\overset{k_{GE}}{\rightleftharpoons}}$ E, where G and E refer to the ground and excited states, respectively, with populations p_G and p_E (= 1 − p_G), and k_{ex} = k_{GE} + k_{EG}. Nonflat relaxation dispersion profiles, with R_2 varying as a function of radio frequency (RF) offset, can be obtained when the spin probes have different chemical shifts in the interconverting states, $\Delta\omega_{GE} = \omega_E - \omega_G \neq 0$ (Figure 1), where ω_i is the chemical shift in state i. For example, in the relatively slow exchange limit, $k_{ex} \leq |\Delta\omega_{GE}|$, the exchange contribution to transverse relaxation is well described by the expression[17]

$$R_{ex} = \frac{p_E(1 - p_E)(\Delta\omega_{GE})^2 k_{ex}}{(\omega_E - \omega_{RF})^2 + \omega_1^2 + k_{ex}^2} \quad (1)$$

so long as the populations of the ground (G) and excited (E) states are highly skewed ($p_E \ll p_G$). In eq 1, ω_{RF} is the carrier position of the RF (amplitude ω_1). Equation 1 establishes that the size of R_{ex} decreases with increasing RF strength, which arises due to a "quenching" of the chemical shift difference, $\Delta\omega_{GE}$.

Equation 1 has been derived for the case where $\Delta\omega_{GE} \neq 0$, $\Delta R_2 = 0$. In what follows, we consider the case where $\Delta R_2 \neq 0$, which is of interest in the applications here. Baldwin and Kay have derived general expressions for R_{ex} (i.e., $\Delta\omega_{GE} \neq 0$, $\Delta R_2 \neq 0$) starting from the complete 6 × 6 Bloch–McConnell exchange matrix[18] (see the Supporting Information); however, the equations are cumbersome and intuition is difficult to obtain.[19] Trott and Palmer have also derived an expression that does not assume $\Delta R_2 = 0$ that is simpler in form.[17] In what follows, we consider a straightforward derivation that provides an expression for R_{ex} that is accurate in the limit where $\omega_1 \gg R_{2,G}$, $R_{2,E}$, k_{ex}, a case that is germane here. As we show below, our approach is particularly useful because it provides a straightforward path for the derivation of additional expressions that provide complementary information to R_{ex} so that complete estimates of exchange parameters can be obtained. For the case where $\omega_1 \gg R_{2,G}$, $R_{2,E}$, k_{ex} the 6 × 6 Bloch–McConnell exchange matrix reduces to a 2 × 2 matrix (see the Supporting Information),

$$\frac{d}{dt}\begin{pmatrix} M_G \\ M_E \end{pmatrix} = \hat{L}\begin{pmatrix} M_G \\ M_E \end{pmatrix}, \quad \hat{L} = \begin{pmatrix} -p_E k_{ex} & (1 - p_E)k_{ex} \\ p_E k_{ex} & -(1 - p_E)k_{ex} - \Delta R_2 \sin^2\theta \end{pmatrix},$$

$$\sin^2\theta = \frac{\omega_1^2}{\omega_1^2 + (\omega_G - \omega_{RF})^2} = \frac{\omega_1^2}{\omega_1^2 + (\omega_E - \omega_{RF})^2} \quad (2)$$

Here we have assumed initially that $\Delta\omega_{GE}$ = 0, that $R_{1,G}$ = $R_{1,E}$ = 0, and that $R_{2,G}$ = 0 so that $R_{2,E}$ = ΔR_2, and θ in eq 2 is the angle between the spin-locked magnetization and the z-axis. Note that $\theta = \theta_G = \theta_E$ when $\Delta\omega_{GE}$ = 0. The solution to this set of equations is

$$M_G(t) = Ae^{\lambda_s t} + Be^{\lambda_f t}$$
$$M_E(t) = Ce^{\lambda_s t} + De^{\lambda_f t} \quad (3)$$

with eigenvalues

DOI: 10.1021/jacs.7b09576
J. Am. Chem. Soc. 2018, 140, 2115–2126

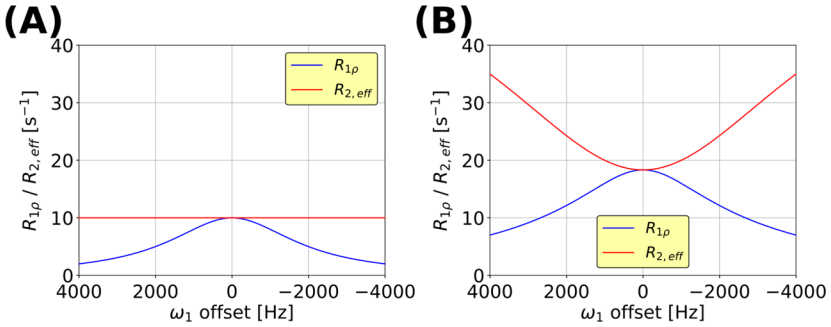

Figure 3. Comparison of $R_{1\rho}$ and R_2 offset profiles in the absence (A) or presence (B) of chemical exchange. The simulations are carried out with the following parameters: k_{ex} = 100 s^{-1}, R_1 = 0 s^{-1}, $R_{2,G}$ = 10 s^{-1}, ΔR_2 = 500 s^{-1}, $\Delta\omega_{GE}$ = 0 and a B_1 field strength of 2000 Hz. Values of p_E = 0 (A) and p_E = 0.10 (B) were used. Note that the $R_{1\rho}$ profile (blue curve) in (B) is shifted vertically from (A) by $p_E \times k_{ex}$ to good approximation for most offsets since ΔR_2 is much larger than k_{ex}.

$$\lambda_{s,f} = \frac{-(k_{ex} + \Delta R_2 \sin^2\theta) \pm \sqrt{(k_{ex} + \Delta R_2 \sin^2\theta)^2 - 4p_E k_{ex}\Delta R_2 \sin^2\theta}}{2} \tag{4}$$

In the case of $p_E \ll 1$, the eigenvalues can be further approximated as

$$\lambda_s \approx -\frac{p_E k_{ex}\Delta R_2 \sin^2\theta}{k_{ex} + \Delta R_2 \sin^2\theta}, \quad \lambda_f \approx -(k_{ex} + \Delta R_2 \sin^2\theta) \tag{5}$$

Similarly, when $\Delta\omega_{GE} \neq 0$, $\theta_G \neq \theta_E$

$$\lambda_s \approx -\frac{p_E k_{ex}\Delta R_2 \sin^2\theta_E + p_E(1-p_E)k_{ex}^2 \sin^2\theta_{EG}}{k_{ex} + \Delta R_2 \sin^2\theta_E},$$
$$\lambda_f \approx -(k_{ex} + \Delta R_2 \sin^2\theta_E) \tag{6}$$

where

$$\sin^2\theta_E = \frac{\omega_1^2}{\omega_1^2 + (\omega_E - \omega_{RF})^2},$$
$$\cos\theta_{EG} = \frac{\omega_1^2 + (\omega_G - \omega_{RF})(\omega_E - \omega_{RF})}{\sqrt{\omega_1^2 + (\omega_G - \omega_{RF})^2}\sqrt{\omega_1^2 + (\omega_E - \omega_{RF})^2}} \tag{7}$$

Since $-\lambda_s$ corresponds to the effective relaxation rate measured as a function of offset in the $R_{1\rho}$ experiment and recalling that $R_{1\rho} = R_1 \cos^2\theta + R_{2,eff} \sin^2\theta$,[2a] where $R_{2,eff} = R_2^o + R_{ex}$ and R_2^o is the intrinsic transverse relaxation rate, it follows that for $\Delta\omega_{GE}$ = 0, $R_{2,G}$ = 0, and R_1 = 0 considered here that

$$R_{ex} = -\lambda_s/\sin^2\theta = \frac{p_E k_{ex}\Delta R_2}{k_{ex} + \Delta R_2 \sin^2\theta} = \frac{1}{\frac{1}{p_E\Delta R_2} + \frac{\sin^2\theta}{p_E k_{ex}}} \tag{8}$$

while for $\Delta\omega_{GE} \neq 0$

$$R_{ex} = -\lambda_s/\sin^2\theta_G = \frac{\omega_{eff,G}^2 + (1-p_E)\Delta\omega_{GE}^2 k_{ex}/\Delta R_2}{\omega_{eff,E}^2/(p_E\Delta R_2) + \omega_1^2/(p_E k_{ex})} \tag{9}$$

where $\omega_{eff,E}^2 = (\omega_E - \omega_{RF})^2 + \omega_1^2$. Equation 9 is identical to more general expressions derived previously by Baldwin and Kay[19] and Trott and Palmer[17] in the limit that $\omega_1 \gg R_{2,G}$, $R_{2,E}$, k_{ex} but the simple approach taken here is used in subsequent derivations below where it is shown that the biphasic decay of the magnetization, eq 3, can be exploited to obtain additional information. It is noteworthy that in the limit where ΔR_2 = 0 eq 9 reduces to

$$R_{ex} = \frac{p_E(1-p_E)\Delta\omega_{GE}^2 k_{ex}}{\omega_{eff,E}^2} \tag{10}$$

that is equivalent to eq 1 for $\omega_1 \gg k_{ex}$, an assumption used in the derivation above (see the Supporting Information).

In Figure 2A $R_{2,eff} - R_1$ is plotted as a function of the offset of the spin-lock field from the ground state resonance position for a number of $\Delta R_2/k_{ex}$ ratios and fixed p_E, k_{ex} and $\Delta\omega_{GE}$, illustrating that the shapes of $R_{1\rho}$-based dispersion profiles depend critically on the relative sizes of ΔR_2 and k_{ex}. Additional profiles are illustrated for the case where $\Delta R_2 > k_{ex}$ in Figure 2B,C. These have been obtained numerically using the full 6 × 6 exchange matrix or via the analytical equations above. The value $R_{2,eff} - R_1$ is plotted along the y-axis that reflects the constant-time based approach that is used to record the relaxation data[20] (see below). Although we have used a large ΔR_2 value (500 s^{-1}) to emphasize the effect in B and C, nonflat dispersion curves can be observed experimentally for ΔR_2 rates as low as 20−30 s^{-1} so long as p_E is large, as shown below. Interestingly, the positions of the minima of the profiles is little influenced by $\Delta\omega_{GE}$ (compare B and C), although for large values of $\Delta\omega_{GE}$ the curves become noticeably asymmetric, as illustrated (Figure 2A or compare $R_{2,eff} - R_1$ values for ω_1 offsets = ± 4000 Hz in C). Panels D−F of Figure 2 illustrate the dependence of $R_{2,eff} - R_1$ on k_{ex} (D), on ΔR_2 (E), and on the offset of the carrier from the resonance position of the spin in question (F) for the case where $\Delta\omega_{GE}$ = 0. Related simulations have been generated by Anthis and Clore who have examined how transverse relaxation rates are influenced by k_{ex} and ΔR_2 in exchanging systems.[21]

In order to obtain a qualitative understanding of the $R_{2,eff} - R_1$ profiles in Figure 2B,C we consider two limiting cases when $\Delta\omega_{GE}$ = 0, with the initial assumption that the spin-locked magnetization is in the transverse plane (θ = 90°). In the case of (i) $\Delta R_2 \gg k_{ex}$, the exchange contribution to R_2 is $p_E \times k_{ex}$, since any magnetization exchanged from the ground state is

DOI: 10.1021/jacs.7b09576
J. Am. Chem. Soc. 2018, 140, 2115−2126

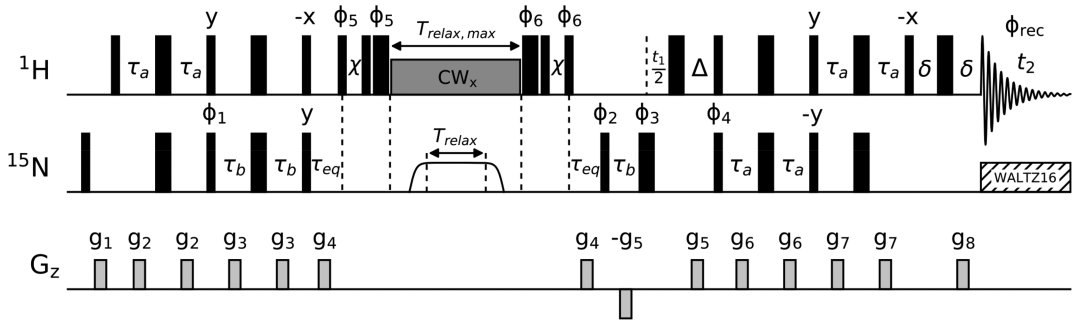

Figure 4. Enhanced sensitivity pulse scheme for measurement of off-resonance ^{15}N $R_{1\rho}$ relaxation rates. All ^{1}H and ^{15}N 90° (180°) RF pulses are shown as narrow (wide) rectangles and are applied at the highest possible power levels. The RF field for the ^{15}N spin-lock was set to ∼2000 Hz and calibrated using an approach described previously.[3] Adiabatic half passage pulses are applied immediately prior to and after the spin-lock element[22] using a tanh/tan shape[25] and a duration of 4 ms. A ^{1}H spin-lock is applied at a field strength of approximately 15 kHz during the $T_{relax,max}$ period (CW_x); simulations have shown that fields as low as ∼8 kHz are sufficient for ^{1}H offsets as large as 2 kHz using typical ^{15}N spin-lock field strengths (1−2 kHz). Note that sample heating is made independent of T_{relax} by applying an ^{15}N spin-lock element for $T_{relax,max} - T_{relax}$ immediately after the t_2 acquisition period. ^{15}N decoupling during acquisition is achieved with a 1.3 kHz WALTZ16 scheme.[26] The ^{1}H carrier is placed on the water signal and moved to the middle of the amide region at the end of the first equilibration period (τ_{eq} value is chosen to ensure that the magnetization components for the exchanging states reflect their equilibrium populations)[27] and subsequently returned to the water frequency at the start of the second τ_{eq} duration. The ^{15}N carrier is placed at the center of the amide region, shifted to the desired offset for the ^{15}N spin-lock at the end of the first equilibration period and subsequently returned back at the start of the second equilibration period. All pulse phases are assumed to be x, unless indicated otherwise. The phase cycling used is $\phi_1 = x, -x$; $\phi_2 = y$; $\phi_3 = 2(x), 2(y), 2(-x), 2(-y)$; $\phi_4 = x$; $\phi_5 = 2(y), 2(-y)$; $\phi_6 = 2(-y), 2(y)$; $\phi_{rec} = x, -x, -x, x$; with a minimum phase cycle of 2. The delays used are $\tau_a = 2.38$ ms, $\tau_b = 1/(4^1J_{HN}) = 2.68$ ms, $\tau_{eq} = (1 - 2)/(k_{ex})$, $\delta = 500$ μs, $\Delta = \tau_b + t_1/2$, $\chi = 1/\omega_{SL} - (4/\pi)$pw, where ω_{SL} is the RF field strength for the ^{1}H spin-lock and pw is the ^{1}H high power 90° pulse width. Gradients are applied with the following durations (ms) and strengths (in % maximum): g_1: (1.0, 15%), g_2: (0.5, 25%), g_3: (0.5, 50%), g_4: (1.0, 70%), g_5: (0.625, 80%), g_6: (0.256, 60%), g_7: (0.256, 15%), g_8: (0.256, 39.6%). Gradients g_5 and g_8 are used for coherence selection and should be optimized to obtain the maximum signal. Weak bipolar gradients (0.3%) are applied during the t_1 evolution period to minimize radiation damping. Quadrature detection in the indirect dimension is obtained using the gradient-based enhanced sensitivity approach[28] by recording two sets of spectra with (ϕ_4, g_8) and ($\phi_4 + \pi$, $-g_8$) for each t_1 increment. The phase ϕ_2 is incremented along with the receiver by 180° for each complex t_1 point.[29]

immediately lost due to the large R_2 of spins in the excited state. In the limit when (ii) $\Delta R_2 \ll k_{ex}$, the increase to the measured R_2 rate from exchange is $\Delta R_2 \times p_E$, which simply reflects the weighted average of R_2 rates for spins exchanging between the ground and excited states. Such results are identical to those obtained in the limit that $\Delta R_2 = 0$ and for nonzero $\Delta\omega_{GE}$, with the roles of $\Delta\omega_{GE}$ and ΔR_2 interchanged in the inequalities above. Next, we consider the offset dependence of $R_{1\rho}$ rates from which R_2 values are derived in an $R_{1\rho}$ experiment (see eqs 8 and 9 above). For simplicity, we assume that $\Delta R_2 \gg k_{ex}$ and that $\Delta\omega_{GE} = 0$. Note that for on-resonance or near on-resonance spin locks, $\Delta R_{1\rho} = \Delta R_2 \times \sin^2\theta \gg k_{ex}$, so that the exchange process in the rotating frame still falls into the "slow" exchange regime. In this case the measured $R_{1\rho}$ rate is increased by $p_E \times k_{ex}$ from exchange. Although $R_{1\rho}$ values are offset independent, R_2 rates will show a distinct dependence from the $\sin^2\theta$ factor that is used to "convert" $R_{1\rho}$ to R_2 in eqs 8 and 9. This accounts for the increase in $R_{2,eff}$ with offset that is observed in panels B and C and for the convex shape of the plots. In the case where the RF offset with respect to the ground state is large so that $\sin^2\theta \approx 0$ then $\Delta R_{1\rho} = \Delta R_2 \times \sin^2\theta \ll k_{ex}$, and the exchange process falls into the "fast" exchange regime. The exchange contribution to $R_{1\rho}$ is thus $\Delta R_{1\rho} \times p_E = \Delta R_2 \times \sin^2\theta \times p_E$, so that the increase in R_2 ($\Delta R_{1\rho} \times p_E/\sin^2\theta$) reaches a maximum value of $\Delta R_2 \times p_E$ as $\sin^2\theta \to 0$. A comparison of $R_{1\rho}$ and $R_{2,eff}$ profiles is presented in Figure 3 where $\Delta\omega_{GE} = 0$, for the case of no exchange (panel A, $p_E = 0$) and where $p_E = 0.1$, $\Delta R_2/k_{ex} > 1$ (panel B).

Figure 4 shows the gradient-based enhanced sensitivity pulse scheme that has been used to record ^{15}N $R_{1\rho}$ relaxation rates. Many of the elements of this experiment are similar to previously published versions,[20,22] and we, therefore, only highlight a number of unique features that will be important in what follows. As described by Palmer and co-workers,[20] a constant-time relaxation element of duration $T_{relax,max}$ is used so that the effective relaxation decay during T_{relax} is given by $(R_{1\rho} - R_1) = (R_{2,eff} - R_1)\sin^2\theta$. Although other sequences have used a small number of ^{1}H 180° pulses during the $T_{relax,max}$ interval to eliminate cross-correlation between ^{1}H−^{15}N dipolar and ^{15}N chemical shift anisotropy relaxation interactions[23] we prefer to apply strong ^{1}H continuous-wave decoupling (∼15 kHz) since large ^{1}H spin flip rates, such as those resulting from solvent exchange,[24] can lead to nonflat R_2 offset dependence profiles even in the absence of chemical exchange. Such artifacts are eliminated by ^{1}H cw decoupling (see the Supporting Information). It is worth noting that a pair of τ_{eq} elements are included whose durations are chosen to be sufficiently long so that magnetization both immediately prior to the start of the T_{relax} period and at the end of $T_{relax,max}$ is at equilibrium ($\tau_{eq} > (1 - 2)/k_{ex}$). This will be become important in what follows.

From the analysis of $R_{1\rho}$ relaxation data recorded with the scheme of Figure 4 it is not possible to extract all of the exchange parameters, even in the relatively simple case where $\Delta\omega_{GE} = 0$, since only the products $p_E \times k_{ex}$ and $p_E \times \Delta R_2$ enter into eq 8. Therefore, only the ratio $k_{ex}/\Delta R_2$ can be quantified from fits of the data. However, an additional constraint can be obtained based on the biexponential decay of spin-locked magnetization (eq 3), which enables the separation of k_{ex} and ΔR_2, hence facilitating the extraction of the complete set of exchange parameters (p_E, k_{ex}, ΔR_2) when ΔR_2 is on the order of or larger than k_{ex}. This "additional information" is accessed in the following way. First, an $R_{1\rho}$ time series is recorded in which spin-lock times, T_{relax}, are chosen such that $|\lambda_f|T_{relax} \gg 1$ so that the fast decaying component is eliminated and the detected signal for a spin probe becomes $\kappa_1\exp(\lambda_s T_{relax})$. This is typically done in any $R_{1\rho}$ analysis since in general $|\lambda_f| \gg |\lambda_s|$. Second, an

DOI: 10.1021/jacs.7b09576
J. Am. Chem. Soc. 2018, 140, 2115−2126

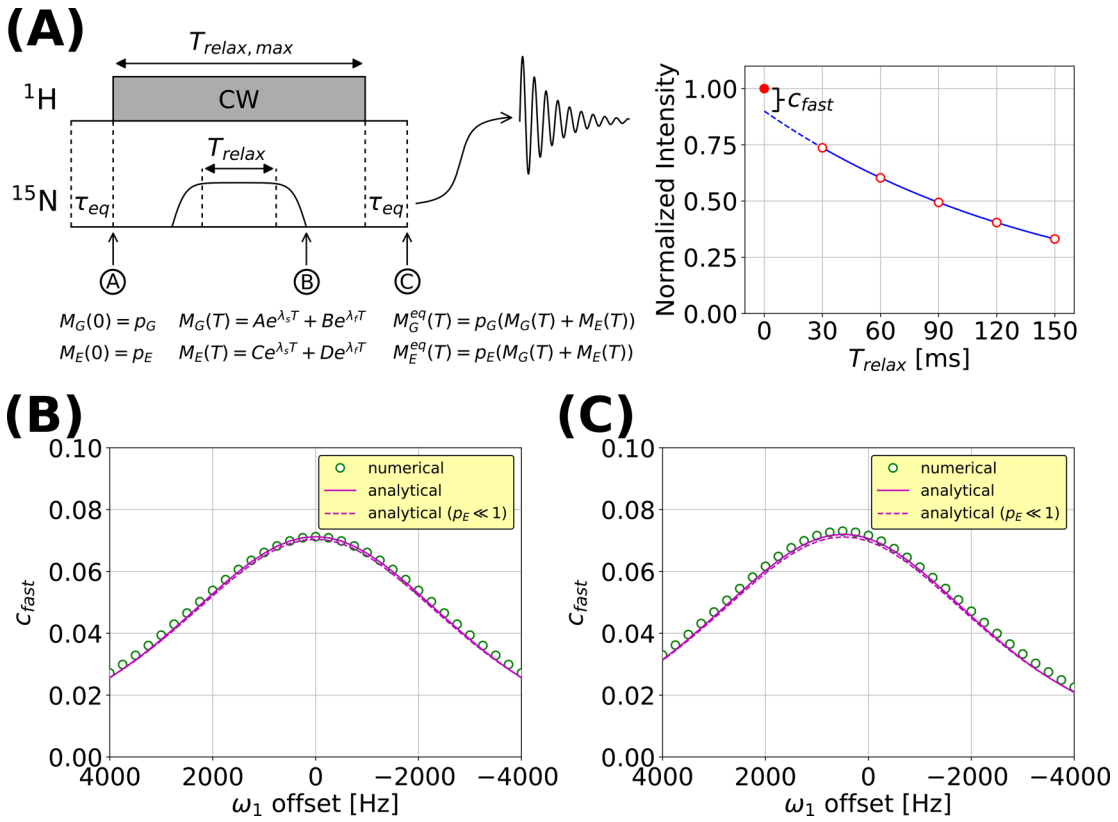

Figure 5. (A) Schematic diagram showing the evolution of magnetization in the ^{15}N $R_{1\rho}$ experiment and the strategy for obtaining c_{fast}. For simplicity, $R_1 = 0$ s^{-1} is assumed. For $T_{relax} \gg 1/|\lambda_f|$ only the A and C terms contribute to observed magnetization so that extrapolation of the exponential fit to the experimental points (open red circles) gives an intercept of $\alpha(A + C)$, where α is a proportionality constant that takes into account the details of magnetization transfer from ^{15}N to ^{1}H. In contrast when an experiment is recorded with $T_{relax} = 0$ (omitting the adiabatic flanking pulses as well) the intensities of correlations are given by $\alpha(A + B + C + D) = \alpha$. In the normalized intensity plot shown c_{fast} is given by $1 - (A + C) = B + D$, or the sum of the coefficients of the fast decaying magnetization component. (B, C) c_{fast} profiles simulated with $p_E = 0.10$, $k_{ex} = 100$ s^{-1}, $R_1 = 0$ s^{-1}, $R_{2,G} = 10$ s^{-1}, $\Delta R_2 = 500$ s^{-1}, B_1 field strength of 2000 Hz, $\Delta\omega_{GE}/(2\pi) = 0$ (B) or 500 Hz (C). Solid and dashed lines in magenta are obtained from analytical equations without or with the assumption of $p_E \ll 1$, respectively.

additional data set is recorded with the spin-lock element removed ($T_{relax} = 0$) so that the magnetization is along the z-axis for the complete $T_{relax,max}$ period, with the detected signal intensity in this case given by κ_2. The ratio $1-\kappa_1/\kappa_2 = B+D$, where B and D are the coefficients of the fast decaying terms in $M_G(t)$ and $M_E(t)$, respectively, eq 3 (see Figure 5A that illustrates this schematically), provides additional information that can be used to obtain unique estimates of p_E, k_{ex} and ΔR_2 on a per-residue basis. The sum $B + D$ (referred to in what follows as c_{fast}) can be readily obtained by solving eq 2 above (see the Supporting Information)

$$B + D = c_{fast} = \frac{p_E \sin^4\theta}{\left(\frac{k_{ex}}{\Delta R_2} + \sin^2\theta\right)^2 - \frac{p_E k_{ex}}{\Delta R_2}\sin^2\theta} \tag{11}$$

and

$$c_{fast} = p_E \frac{[(\Delta R_2 \sin^2\theta_E) + (1 - p_E)k_{ex}(1 - \cos\theta_{EG})]^2 + p_E(1 - p_E)k_{ex}^2(1 - \cos\theta_{EG})^2}{(k_{ex} + \Delta R_2 \sin^2\theta_E)^2 - p_E k_{ex}\Delta R_2 \sin^2\theta_E - p_E(1 - p_E)k_{ex}^2 \sin^2\theta_{EG}} \tag{12}$$

for $\Delta\omega_{GE} = 0$ (eq 11) and $\Delta\omega_{GE} \neq 0$ (eq 12). Figures 5B,C illustrate the offset dependence of c_{fast} for $\Delta\omega_{GE} = 0$ (B) and $\Delta\omega_{GE} \neq 0$ (C). Notably, unlike the offset dependence of $R_{1\rho} - R_1$, the extremum of the c_{fast} profile is shifted to the resonance position of the excited state. However, for small values of $\Delta\omega_{GE}$, as for Ddx4 ($|\Delta\varpi_{GE}| < 0.2$ ppm, see below), the shifts are very small and hence difficult to observe (or quantify).

Application to the Ddx4 Phase-Separating Protein. Many compartments in the cell are sequestered via membranes, however the cell also concentrates molecules such as proteins and nucleic acids into membraneless organelles that are stabilized through an array of intermolecular interactions.[8d,30] Such membraneless structures are involved in a variety of different biochemical processes including RNA processing and signaling.[8a−c] The intrinsically disordered region of Ddx4, a major component of germ granules,[6] phase separates to form a highly concentrated protein phase of approximately 400 mg/mL,[7] and many other examples of phase-separating IDPs have been reported in the literature.[31] However, relatively little is known quantitatively about the forces that drive phase separation and about the structural and dynamical properties of the phase-separated protein molecules. We have used Ddx4$_{1-236}$ as a model system in an attempt to characterize in more detail what the driving forces might be.

DOI: 10.1021/jacs.7b09576
J. Am. Chem. Soc. 2018, 140, 2115−2126

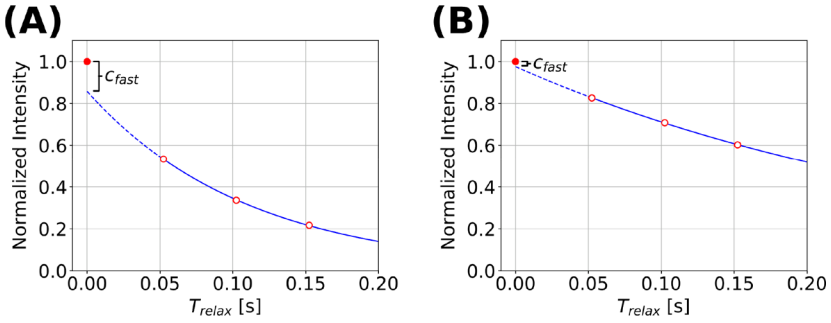

Figure 6. Representative experimental ^{15}N $R_{1\rho}$ decay curves (open red circles) and fits (blue solid curves) for a backbone amide from Ddx4$_{cond}$. (A) $R_{1\rho}$ decay curve when the ^{15}N carrier is on-resonance and (B) off-resonance by 3000 Hz. $R_{1\rho}$ values are obtained by fitting all points except for T_{relax} = 0 (solid red circle) to a single-exponential decay function. Measurement errors are smaller than the size of the dots. Note that T_{relax} values (except for T_{relax} = 0) have been corrected for the duration of the adiabatic half passage pulses as described in the Supporting Information.

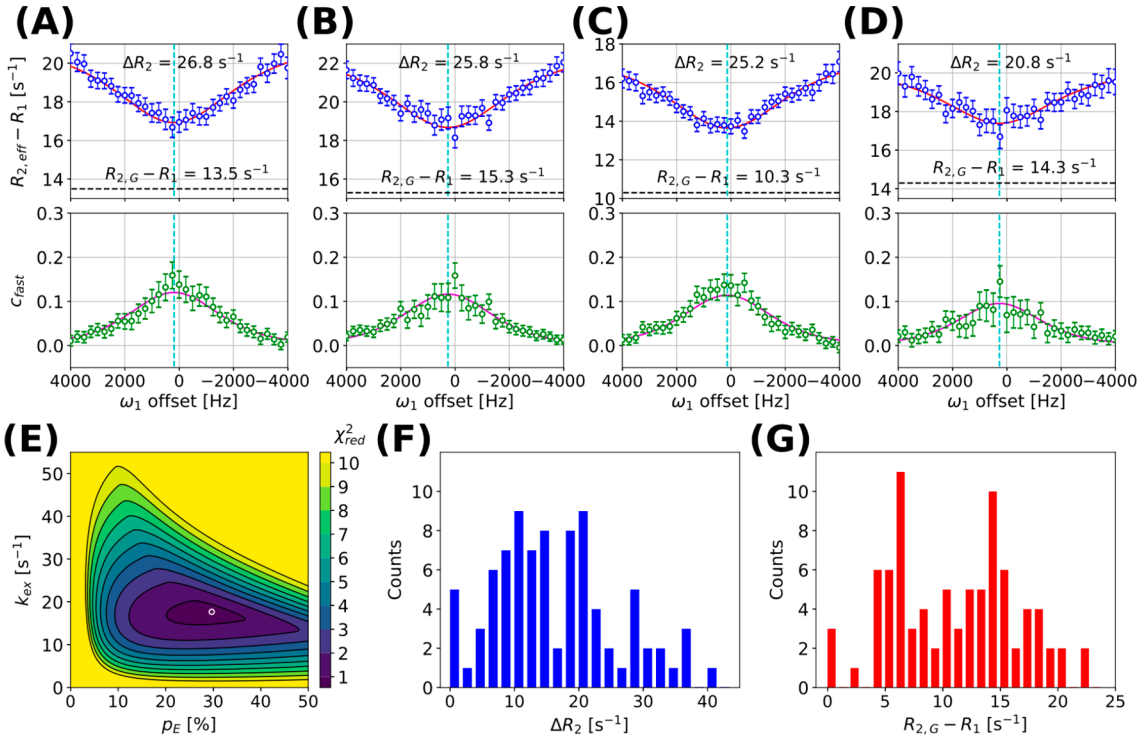

Figure 7. Representative experimental ^{15}N $R_{1\rho}$ profiles from Ddx4$_{cond}$. (A–D) $R_{2,eff} - R_1$ dispersion (blue circles) and corresponding c_{fast} profiles (green circles), along with best fits using the analytical expressions in the text without the assumption of $p_E \ll 1$. All fits assumed that $\Delta\omega_{GE}$ = 0; simulations have shown that this does not introduce significant errors into extracted exchange parameters or ΔR_2 values, even in cases of large shift differences, although χ^2 values do increase. The dashed lines in cyan (vertical) and black (horizontal) denote the chemical shift of the ground state (0 Hz corresponds to 118 ppm, the center of the spectrum) and the intrinsic $R_{2,G} - R_1$ rate in the absence of slow exchange obtained from the analytical curve fitting, respectively. The four residues selected correspond to 15, 16, 17, and 26 in Figure S7A. Note that maxima in c_{fast} profiles are not displaced from the resonance positions of the ground state because $|\Delta\omega_{GE}|$ values are very small (see text). (E) χ^2 surface showing the optimal (p_E, k_{ex}) for Ddx4$_{cond}$ from the global fit, (29.7%, 17.7 s^{-1}), as indicated by the white circle in the plot. Histograms of ΔR_2 (F) and $R_{2,G} - R_1$ (G) values are illustrated, obtained from fits of 86 dispersion profiles with values of (p_E, k_{ex}) fixed to (29.7%, 17.7 s^{-1}).

Several lines of evidence suggest that molecules of Ddx4$_{1-236}$ interact in the condensed phase. First, there are large numbers of intermolecular NOEs in samples prepared with 10% [U-^{15}N,^{13}C]-labeled, 90% unlabeled Ddx4$_{1-236}$, a clear indication of interactions between adjacent chains.[7b] Second, the hydrodynamic radius of Ddx4$_{1-236}$ has been measured from NMR diffusion experiments to be 32 Å[7b] that is much closer to the value predicted for a folded protein of the same number of amino acids (23 Å) than for an unfolded protein (50 Å).[32] For a relatively compact protein, such as Ddx4$_{1-236}$, the concentration (C^*) at which the protein molecules become in contact with each other (corresponding to the transition from a dilute to a semidilute solution) can be estimated from the relation

$$C^* = \frac{3MW}{4\pi N_a R_H^3} \quad (13)$$

where MW and R_H are the protein molecular weight and hydrodynamic radius, respectively, and N_a is Avogadro's number.[33] Using the measured R_H value of 31.6 Å for Ddx4$_{1-236}$,[7b] C^* is calculated to be approximately 325 mg/mL, similar to the protein concentration in the condensed phase of phase-separated Ddx4$_{1-236}$, Ddx4$_{cond}$ (380 mg/mL). Ddx4$_{cond}$ is thus expected to approximate a semidilute protein

DOI: 10.1021/jacs.7b09576
J. Am. Chem. Soc. 2018, 140, 2115–2126

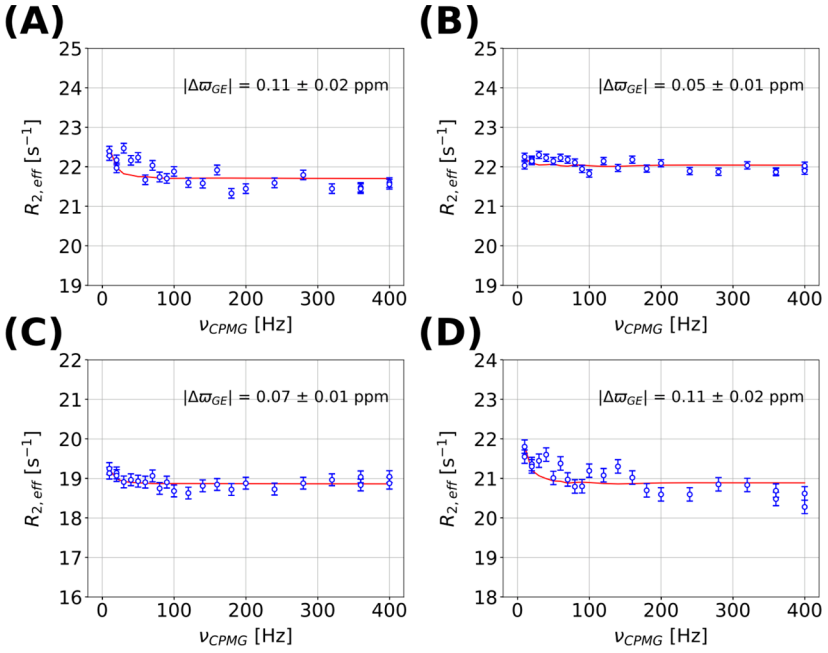

Figure 8. ^{15}N CPMG profiles measured with the sequence of Yang and co-workers[13] of the same Ddx4$_{cond}$ residues as in Figure 7. $|\Delta\varpi_{GE}|$ values were obtained with (p_E, k_{ex}, ΔR_2) fixed from fits of ^{15}N off-resonance $R_{1\rho}$ curves. The red lines are obtained from a global fit using the program ChemEx.[16]

solution in which the protein molecules partially overlap with one another, leading to transient intermolecular contacts.

In an attempt to characterize such interactions we have carried out an off-resonance ^{15}N $R_{1\rho}$ study of Ddx4$_{cond}$, using the pulse scheme of Figure 4. Figure 6A,B illustrates a representative pair of $R_{1\rho} - R_1$ decay profiles recorded for one residue from Ddx4$_{cond}$ with RF offsets of 0 (A) and 3 kHz (B) from the ground state resonance position. In addition to obtaining measurements for T_{relax} values of 50, 100, and 150 ms (open red circles), we have also recorded a spectrum with the spin-lock element omitted so that the magnetization resides along the z-axis for the duration of the $T_{relax,max}$ period (solid red circle at $T_{relax} = 0$). All intensities have been normalized so that the point at $T_{relax} = 0$ is set to 1. Exponential fits of the 3 points with T_{relax} values ranging from 50 to 150 ms are shown in blue and the difference between the solid red circle and the corresponding position of the exponential function at $T_{relax} = 0$ (extrapolated value, dashed blue curve) gives c_{fast}. Note that the $R_{1\rho}$ profiles clearly indicate that magnetization decay is not single-exponential (when the $T_{relax} = 0$ point is considered), as expected from eq 3.

Figure 7A–D shows four representative $R_{2,eff} - R_1$ dispersion profiles (blue circles) and the corresponding c_{fast} curves (green circles), along with fits of the experimental data to analytical expressions that do not make the assumption of $p_E \ll 1$ (solid curves). Additional profiles are shown in Supporting Information. Note that the ω_1 offset, plotted along the x-axis, refers to the offset of the RF from the center of the spectrum (118 ppm), and not from the position of the ground state resonance. Cyan dashed lines indicate the resonance offset of each ground state peak (in Hz) with respect to 118 ppm. As discussed above, it is possible to extract per-residue values of (p_E, k_{ex}, ΔR_2) from each $R_{2,eff} - R_1$, c_{fast} pair of profiles. The similar values of p_E and k_{ex} for residues analyzed individually in initial fits (mean and standard deviation for p_E and k_{ex} of 35.3 ± 13.0% and 18.4 ± 2.3 s^{-1}, respectively) indicated that a global fit of the data could be performed. In total data from 26 residues were included in the initial analysis, corresponding to those amides with high quality $R_{2,eff} - R_1$ profiles that vary by at least 2 s^{-1} over the complete range of offset values recorded (Supporting Information). Values for (p_E, k_{ex}) of (29.7%, 17.7 s^{-1}) were fit, Figure 7E. The extracted rates, ΔR_2 and $R_{2,G} - R_1$, for these 26 residues when fit globally range between 14.5 and 40.5 s^{-1} (24.5 ± 6.7 s^{-1}) and 0.1–15.3 s^{-1} (8.3 ± 4.1 s^{-1}) respectively, and $R_{2,E} = (4.5 \pm 2.7) \times R_{2,G}$. Panels F and G of Figure 7 show histograms of residue specific ΔR_2 and $R_{2,G} - R_1$ values, respectively, from the analysis of 86 off-resonance $R_{1\rho}$ dispersion profiles (Supporting Information). Notably, and as expected, the exchange-free measures of $R_{2,G}$ obtained in the present analysis are up to 4.6 s^{-1} smaller than $R_{2,G}$ values measured from on-resonance $R_{1\rho}$ experiments that have been reported previously,[7b] with an average decrease of 2.5 ± 1.0 s^{-1}. In that study we calculated an average dynamics parameter, $\langle S^2\tau_c \rangle$ = 8.5 ns (where S^2 is the backbone amide order parameter squared and τ_c is the assumed isotropic correlation time) for Ddx4$_{cond}$ and based on the revised exchange-free measures of $R_{2,G}$ obtained here we estimate that this parameter should be decreased by approximately 17%, with no change to any of the conclusions from that work.

In addition to the exchange parameters discussed above, we were interested in estimating the chemical shift differences between amide nitrogens in the ground and excited states, $\Delta\omega_{GE}$, as well. These can, in principle, be obtained from c_{fast} profiles, since as described above, extrema are shifted to the positions of the excited state resonances. In practice, however, this is very difficult to achieve for small $|\Delta\omega_{GE}|$ values, and in the case of Ddx4$_{cond}$ essentially no shifts were observed (Figure 7). We therefore recorded an ^{15}N CPMG relaxation dispersion experiment on a sample of Ddx4$_{cond}$, using a large constant-time relaxation delay, T_{relax} = 100 ms, in order to focus on the initial region of the CPMG curve corresponding to low CPMG pulsing frequencies, ν_{CPMG}. This is essential in studies of

DOI: 10.1021/jacs.7b09576
J. Am. Chem. Soc. 2018, 140, 2115–2126

systems with very small k_{ex} rates, where profiles are likely to be small and rapidly quenched as a function of ν_{CPMG}. Dispersion profiles were obtained starting from ν_{CPMG} values as low as 10 Hz that were quenched by $\nu_{CPMG} \approx 50$ Hz, as shown in Figure 8 where relaxation data are displayed for the same residues whose $R_{1\rho}$ profiles are shown in Figure 7. The CPMG data were fit globally to a model of two-site exchange enforcing (p_E, k_{ex}, and ΔR_2) to values determined from the $R_{1\rho}$, c_{fast} set of experiments (red solid curves). Notably, the extracted chemical shift differences are small, < 0.2 ppm. Although the exchange parameters are within a window that is amenable for study by CEST,[34] we were not able to observe distinct dips from the excited state in ^{15}N CEST profiles recorded using a weak B_1 field of ∼30 Hz, a result that is consistent with the small $|\Delta\omega_{GE}|$ values obtained in the CPMG study.

The relaxation data thus paint a picture whereby Ddx4 molecules in Ddx4$_{cond}$ exchange between a ground state and a significantly populated excited state ($p_E \approx 0.3$) involving intermolecular interactions that are most likely weak and transiently formed, as little changes to ^{15}N chemical shifts were measured between the two states. The increase in $R_{2,E}$ values (relative to $R_{2,G}$ rates) is consistent with increased interactions in the excited state that reduce correlation times for the affected regions leading to faster relaxation. The results add to our previous NOE studies of the ground state,[7b] pointing to an even more extensive set of intermolecular interactions in the excited state ensemble.

Next we examined a mutant of Ddx4$_{1-236}$ in which all 14 Phe residues have been replaced by Ala, Ddx4$_{14FtoA}$ (see Materials and Methods). We had previously shown that at temperatures above 5 °C Ddx4$_{14FtoA}$ is not able to phase separate.[7b] Notably, however, high concentrations of Ddx4$_{14FtoA}$ can be produced (∼400 mg/mL) through extensive centrifugation, as opposed to spontaneously through phase separation in the case of Ddx4$_{cond}$. An extensive network of intermolecular NOEs was observed previously in samples of Ddx4$_{14FtoA}$ (370 mg/mL), similar to that for Ddx4$_{cond}$, suggesting that an analogous exchange process as observed for Ddx4$_{cond}$ might be present for the mutant at high protein concentrations as well. In order to explore this possibility we performed similar off-resonance $R_{1\rho}$ experiments on a 370 mg/mL sample of Ddx4$_{14FtoA}$ and as illustrated in Supporting Information, dispersion profiles of similar magnitudes to those measured for the wild-type protein were noted that establish a slow time-scale exchange process in the mutant protein as well ((p_E, k_{ex}) = (25.2%, 23.1 s^{-1})). Although the observed slow conformational dynamics are not unique to the phase-separated Ddx4 state it is important to realize that the high protein concentrations that are required for conformational exchange (see below) can only be generated spontaneously by phase separation; highly concentrated samples of Ddx4$_{14FtoA}$ are only produced artificially through extensive centrifugation.

If the small but quantifiable $R_{1\rho}$ dispersion profiles observed for both Ddx4 samples discussed above derive from contacts between neighboring Ddx4 molecules in highly concentrated protein solutions (∼400 mg/mL) then these profiles should become flat as the protein concentration is reduced. We have therefore repeated experiments using a sample of Ddx4$_{14FtoA}$ at a protein concentration of 2 mM and flat profiles were indeed obtained (see Supporting Information). As a further control, we have also recorded $R_{1\rho}$ experiments on a sample of protein L, that is not expected to have measurable exchange, and flat profiles were obtained in this case as well (Supporting Information).

The fact that dispersion effects can be observed and quantified for systems with little or no change in chemical shifts between states and where ΔR_2 values are only 20−30 s^{-1} is the central result of this work. In this regard the $R_{1\rho}$, c_{fast} approach described here provides a unique window into an exchange regime that has not been studied extensively to date. Finally, the impressive sensitivity of the off-resonance $R_{1\rho}$ method to exchange processes with small ΔR_2 and k_{ex} values notwithstanding, it remains the case that the robust estimation of exchange parameters does place certain constraints on exchange rates. For example, as described above, care must be taken to ensure that magnetization immediately prior to the start of the spin-lock relaxation element and at the end of the $T_{relax,max}$ period (see Figures 4 and 5A) reports faithfully on the equilibrium populations of the exchanging states and values of T_{relax} must be chosen such that $|\lambda_f|T_{relax} \gg 1$ (Figures 4 and 5A). In this context it is worth noting that the small k_{ex} values for Ddx4$_{cond}$ and Ddx4$_{14FtoA}$ challenge the robust estimation of exchange parameters because it is difficult to choose appropriate values of T_{relax} without significantly affecting the sensitivity of the experiments (here T_{relax} = 50, 100, and 150 ms were used). Simulations that we have performed using the fitted (p_E, k_{ex}, ΔR_2) values along with the T_{relax} values used in our measurements suggest that k_{ex} (∼18 s^{-1}) is likely to be slightly overestimated and, notably, a value of approximately 12 s^{-1} is obtained when the first T_{relax} point (50 ms) is removed from analysis, with relatively minor changes to p_E and ΔR_2. Moreover, additional simulations suggest that the most sensitive exchange window lies in a regime where $k_{ex} \sim \Delta R_2$, on the order of 50−100 s^{-1} (or larger).

Comparison with DEST. It is worth noting that the approach described here for studying slowly exchanging systems is similar in many respects to the elegant DEST experiment developed by Clore and co-workers.[5,35] DEST, as it has been used presently, focuses on exchanging systems where $R_{2,E}$ is very large (typically many thousands of s^{-1}) and exploits a relatively weak field applied over a large frequency range, $\Delta R_2 \gg \omega_1$. In contrast, the $R_{1\rho}$ methodology described here uses a larger RF field applied over a narrower frequency window since ΔR_2 rates are much smaller. Notably, in the limit where $\omega_1 \gg R_{2,E}$, $R_{2,G}$ and $\omega_1 \gg k_{ex}$, as in the present application, the 6 × 6 exchange matrix can be reduced to a simple 2 × 2 form, to good accuracy (see above); the resulting equations establish that it is not possible to separate p_E from k_{ex} and ΔR_2. Further, in this limit additional information is not obtained by recording multiple $R_{1\rho}$ profiles with different RF strengths (see eq S10). Thus, in studies of systems where ΔR_2 is relatively small additional experiments, such as recording c_{fast}, are required to obtain p_E, k_{ex} and ΔR_2. This is in contrast to DEST studies on exchanging protein systems with large ΔR_2 values and for which $\Delta R_2 \gg \omega_1$. Here simulations that we have done show that it remains advantageous to record a pair of data sets with different ω_1 values[5] that, in principle, when fit together enable the separation of all exchange parameters. The DEST and $R_{1\rho}$, c_{fast} experiments are thus complementary, focusing on applications to exchanging systems with very different ΔR_2 rates.

CONCLUDING REMARKS

Herein, we have presented an off-resonance $R_{1\rho}$, c_{fast} experiment for the study of slowly exchanging protein systems, with ΔR_2 on the order of, or greater than, k_{ex}. Interestingly, R_2 vs ω_1

DOI: 10.1021/jacs.7b09576
J. Am. Chem. Soc. 2018, 140, 2115−2126

offset profiles are inverted relative to the characteristic shapes that are obtained in the more studied case where $\Delta\omega_{GE} \neq 0$, $\Delta R_2 \sim 0$. A set of equations is derived, based on simplifications to the exchange matrix, that is valid in the limit of $\omega_1 \gg R_{2,E}$, $R_{2,G}$ and $\omega_1 \gg k_{ex}$. The solution of the resulting exchange equations predicts the experimentally observed dispersion profiles as well as the c_{fast} offset dependence that is required for separation of the exchange parameters. We show that it is possible to extract a complete set of exchange parameters, even for the case where dispersion profiles are relatively small (2 s^{-1}) and when ΔR_2 values are only 20−30 s^{-1} so long as p_E values are reasonably large (>0.1). It is anticipated that the method will be of utility in studies of weakly or transiently interacting systems where small chemical shift changes are often the norm, but with potentially significant ΔR_2 values. Other approaches such as CEST, while suited for studies of interconverting systems in slow exchange,[4,34] may fail in cases when $|\Delta\varpi| \leq$ 0.2−0.3 ppm (^{15}N), while the $R_{1\rho}$, c_{fast} approach remains viable even when $\Delta\varpi = 0$. An application to the study of exchange in $Ddx4_{cond}$ is presented, showing that Ddx4 molecules exchange between a pair of states, where the excited conformer is significantly populated ($p_E \approx 0.3$) with increased intermolecular interactions that lead to more rapid transverse relaxation. Further applications to more complex, multicomponent phase separated systems, as found in typical membraneless organelles, will help clarify how interactions between neighboring protein molecules are modulated, leading to a greater understanding of the relation between dynamics and function in these important biological complexes.

■ ASSOCIATED CONTENT

Supporting Information

The Supporting Information is available free of charge on the ACS Publications website at DOI: 10.1021/jacs.7b09576.

Additional theoretical discussion of the $R_{1\rho}$ experiment, including experimental details, pulse sequence code, and Figures S1−S7 (PDF)

■ AUTHOR INFORMATION

Corresponding Author

*kay@pound.med.utoronto.ca

ORCID

Tairan Yuwen: 0000-0003-3504-7995

Lewis E. Kay: 0000-0002-4054-4083

Notes

The authors declare no competing financial interest.

■ ACKNOWLEDGMENTS

We are grateful to Dr. Ashok Sekhar for valuable discussions and contributions at an early phase of this work. This research was supported by grants from the Canadian Institutes of Health Research and the Natural Sciences and Engineering Research Council of Canada. L.E.K. holds a Canada Research Chair in Biochemistry.

■ REFERENCES

(1) (a) Karplus, M.; Kuriyan, J. *Proc. Natl. Acad. Sci. U. S. A.* **2005**, *102*, 6679−6685. (b) Sekhar, A.; Kay, L. E. *Proc. Natl. Acad. Sci. U. S. A.* **2013**, *110*, 12867−12874. (c) Henzler-Wildman, K.; Kern, D. *Nature* **2007**, *450*, 964−972.

(2) (a) Palmer, A. G.; Kroenke, C. D.; Loria, J. P. *Methods Enzymol.* **2001**, *339*, 204−238. (b) Neudecker, P.; Robustelli, P.; Cavalli, A.; Walsh, P.; Lundstrom, P.; Zarrine-Afsar, A.; Sharpe, S.; Vendruscolo, M.; Kay, L. E. *Science* **2012**, *336*, 362−366. (c) Korzhnev, D. M.; Religa, T. L.; Banachewicz, W.; Fersht, A. R.; Kay, L. E. *Science* **2010**, *329*, 1312−1316. (d) Eisenmesser, E. Z.; Millet, O.; Labeikovsky, W.; Korzhnev, D. M.; Wolf-Watz, M.; Bosco, D. A.; Skalicky, J. J.; Kay, L. E.; Kern, D. *Nature* **2005**, *438*, 117−121. (e) Boehr, D. D.; McElheny, D.; Dyson, H. J.; Wright, P. E. *Science* **2006**, *313*, 1638−1642. (f) Whittier, S. K.; Hengge, A. C.; Loria, J. P. *Science* **2013**, *341*, 899−903. (g) Libich, D. S.; Tugarinov, V.; Clore, G. M. *Proc. Natl. Acad. Sci. U. S. A.* **2015**, *112*, 8817−8823.

(3) Palmer, A. G.; Massi, F. *Chem. Rev.* **2006**, *106*, 1700−1719.

(4) Vallurupalli, P.; Bouvignies, G.; Kay, L. E. *J. Am. Chem. Soc.* **2012**, *134*, 8148−8161.

(5) Fawzi, N. L.; Ying, J. F.; Ghirlando, R.; Torchia, D. A.; Clore, G. M. *Nature* **2011**, *480*, 268−272.

(6) (a) Kotaja, N.; Sassone-Corsi, P. *Nat. Rev. Mol. Cell Biol.* **2007**, *8*, 85−90. (b) Raz, E. *Genome Biol.* **2000**, *1*, 1017.1−1017.6.

(7) (a) Nott, T. J.; Petsalaki, E.; Farber, P.; Jervis, D.; Fussner, E.; Plochowietz, A.; Craggs, T. D.; Bazett-Jones, D. P.; Pawson, T.; Forman-Kay, J. D.; Baldwin, A. J. *Mol. Cell* **2015**, *57*, 936−947. (b) Brady, J. P.; Farber, P.; Sekhar, A.; Lin, Y.; Rui, H.; Bah, A.; Nott, T. J.; Chan, H.; Baldwin, A. J.; Forman-Kay, J.; Kay, L. E. *Proc. Natl. Acad. Sci. U. S. A.* **2017**, *114*, E8194−E8203.

(8) (a) Li, P. L.; Banjade, S.; Cheng, H. C.; Kim, S.; Chen, B.; Guo, L.; Llaguno, M.; Hollingsworth, J. V.; King, D. S.; Banani, S. F.; Russo, P. S.; Jiang, Q. X.; Nixon, B. T.; Rosen, M. K. *Nature* **2012**, *483*, 336−340. (b) Anderson, P.; Kedersha, N. *Nat. Rev. Mol. Cell Biol.* **2009**, *10*, 430−436. (c) Sheth, U.; Parker, R. *Science* **2003**, *300*, 805−808. (d) Banani, S. F.; Lee, H. O.; Hyman, A. A.; Rosen, M. K. *Nat. Rev. Mol. Cell Biol.* **2017**, *18*, 285−298.

(9) Mulder, F. A. A.; Skrynnikov, N. R.; Hon, B.; Dahlquist, F. W.; Kay, L. E. *J. Am. Chem. Soc.* **2001**, *123*, 967−975.

(10) Korzhnev, D. M.; Salvatella, X.; Vendruscolo, M.; Di Nardo, A. A.; Davidson, A. R.; Dobson, C. M.; Kay, L. E. *Nature* **2004**, *430*, 586−590.

(11) Palmer, A. G. *J. Magn. Reson.* **2014**, *241*, 3−17.

(12) (a) Mittermaier, A.; Kay, L. E. *J. Am. Chem. Soc.* **2001**, *123*, 6892−6903. (b) Bouvignies, G.; Kay, L. E. *J. Biomol. NMR* **2012**, *53*, 303−310.

(13) Jiang, B.; Yu, B. H.; Zhang, X.; Liu, M. L.; Yang, D. W. *J. Magn. Reson.* **2015**, *257*, 1−7.

(14) Delaglio, F.; Grzesiek, S.; Vuister, G. W.; Zhu, G.; Pfeifer, J.; Bax, A. *J. Biomol. NMR* **1995**, *6*, 277−293.

(15) Press, W. H.; Teukolsky, S. A.; Vetterling, W. T.; Flannery, B. P. *Numerical Recipes in C*, 2 ed.; Cambridge University Press: Cambridge, 1998.

(16) https://github.com/gbouvignies/chemex.

(17) Trott, O.; Palmer, A. G. *J. Magn. Reson.* **2002**, *154*, 157−160.

(18) McConnell, H. M. *J. Chem. Phys.* **1958**, *28*, 430−431.

(19) Baldwin, A. J.; Kay, L. E. *J. Biomol. NMR* **2013**, *55*, 211−218.

(20) Akke, M.; Palmer, A. G. *J. Am. Chem. Soc.* **1996**, *118*, 911−912.

(21) Anthis, N. J.; Clore, G. M. *Q. Rev. Biophys.* **2015**, *48*, 35−116.

(22) Mulder, F. A. A.; de Graaf, R. A.; Kaptein, R.; Boelens, R. *J. Magn. Reson.* **1998**, *131*, 351−357.

(23) Korzhnev, D. M.; Skrynnikov, N. R.; Millet, O.; Torchia, D. A.; Kay, L. E. *J. Am. Chem. Soc.* **2002**, *124*, 10743−10753.

(24) Yuwen, T.; Skrynnikov, N. R. *J. Magn. Reson.* **2014**, *241*, 155−169.

(25) Baum, J.; Tycko, R.; Pines, A. *Phys. Rev. A: At., Mol., Opt. Phys.* **1985**, *32*, 3435−3447.

(26) Shaka, A. J.; Keeler, J.; Frenkiel, T.; Freeman, R. *J. Magn. Reson.* **1983**, *52*, 335−338.

(27) Hansen, D. F.; Vallurupalli, P.; Kay, L. E. *J. Phys. Chem. B* **2008**, *112*, 5898−5904.

(28) (a) Kay, L. E.; Keifer, P.; Saarinen, T. *J. Am. Chem. Soc.* **1992**, *114*, 10663−10665. (b) Schleucher, J.; Sattler, M.; Griesinger, C. *Angew. Chem., Int. Ed. Engl.* **1993**, *32*, 1489−1491.

(29) Marion, D.; Ikura, M.; Tschudin, R.; Bax, A. *J. Magn. Reson.* **1989**, *85*, 393−399.

DOI: 10.1021/jacs.7b09576
J. Am. Chem. Soc. 2018, 140, 2115−2126

(30) (a) Toretsky, J. A.; Wright, P. E. *J. Cell Biol.* **2014**, *206*, 579−588. (b) Hyman, A. A.; Weber, C. A.; Juelicher, F. *Annu. Rev. Cell Dev. Biol.* **2014**, *30*, 39−58. (c) Mitrea, D. M.; Kriwacki, R. W. *Cell Commun. Signaling* **2016**, *14*, 1. (d) Chong, P. A.; Forman-Kay, J. D. *Curr. Opin. Struct. Biol.* **2016**, *41*, 180−186.
(31) (a) Burke, K. A.; Janke, A. M.; Rhine, C. L.; Fawzi, N. L. *Mol. Cell* **2015**, *60*, 231−241. (b) Conicella, A. E.; Zerze, G. H.; Mittal, J.; Fawzi, N. L. *Structure* **2016**, *24*, 1537−1549. (c) Hough, L. E.; Dutta, K.; Sparks, S.; Temel, D. B.; Kamal, A.; Tetenbaum-Novatt, J.; Rout, M. P.; Cowburn, D. *eLife* **2015**, *4*, No. e10027. (d) Elbaum-Garfinkle, S.; Kim, Y.; Szczepaniak, K.; Chen, C. C. H.; Eckmann, C. R.; Myong, S.; Brangwynne, C. P. *Proc. Natl. Acad. Sci. U. S. A.* **2015**, *112*, 7189−7194. (e) Mitrea, D. M.; Cika, J. A.; Guy, C. S.; Ban, D.; Banerjee, P. R.; Stanley, C. B.; Nourse, A.; Deniz, A. A.; Kriwacki, R. W. *eLife* **2016**, *5*, No. e13571. (f) Strom, A. R.; Emelyanov, A. V.; Mir, M.; Fyodorov, D. V.; Darzacq, X.; Karpen, G. H. *Nature* **2017**, *547*, 241−245.
(32) Wilkins, D. K.; Grimshaw, S. B.; Receveur, V.; Dobson, C. M.; Jones, J. A.; Smith, L. J. *Biochemistry* **1999**, *38*, 16424−16431.
(33) Mohr, P. J.; Taylor, B. N.; Newell, D. B. *Rev. Mod. Phys.* **2012**, *84*, 1527−1605.
(34) Vallurupalli, P.; Sekhar, A.; Yuwen, T.; Kay, L. E. *J. Biomol. NMR* **2017**, *67*, 243−271.
(35) (a) Fawzi, N. L.; Libich, D. S.; Ying, J. F.; Tugarinov, V.; Clore, G. M. *Angew. Chem., Int. Ed.* **2014**, *53*, 10345−10349. (b) Fawzi, N. L.; Ying, J. F.; Torchia, D. A.; Clore, G. M. *Nat. Protoc.* **2012**, *7*, 1523−1533.

DOI: 10.1021/jacs.7b09576
J. Am. Chem. Soc. 2018, 140, 2115−2126